Perspective

Fast Electron Tomography for Nanomaterials

Wiebke Albrecht and Sara Bals*

ACCESS | Metrics & More | Article Recommendations

ABSTRACT: Electron tomography (ET) has become a well-established technique to visualize nanomaterials in three dimensions. A vast richness in information can be gained by ET, but the conventional acquisition of a tomography series is an inherently slow process on the order of 1 h. The slow acquisition limits the applicability of ET for monitoring dynamic processes or visualizing nanoparticles, which are sensitive to the electron beam. In this Perspective, we summarize recent work on the development of emerging experimental and computational schemes to enhance the data acquisition process. We particularly focus on the application of these fast ET techniques for beam-sensitive materials and highlight insight into dynamic transformations of nanoparticles under external stimuli, which could be gained by fast in situ ET. Moreover, we discuss challenges and possible solutions for simultaneously increasing the speed and quality of fast ET.

INTRODUCTION

The rapid development in the synthesis of new nanomaterials leading to complex nanoparticle (NP) morphologies[1−3] and possibly consisting of several elements[4,5] has driven the development of novel characterization techniques at a high spatial resolution. Although transmission electron microscopy (TEM) is a powerful tool for determining the structural properties of NPs, it only provides two-dimensional (2D) projection images of the analyzed objects.[6] Hence, electron tomography (ET) has become a standard technique to assess the three-dimensional (3D) morphology and interior structure of NPs.[7−9] Currently, it has provided valuable insight for material science, such as elucidating the origin of chirality in NPs,[3,10] determining the influence of planar defects and seed location on the growth of NPs,[11,12] and even unravelling the atomic structure of nanomaterials.[13−15] When combined with spectroscopic techniques such as energy-dispersive X-ray spectroscopy (EDXS) or electron energy loss spectroscopy (EELS), additional information about the 3D elemental composition,[16,17] oxidation state,[18,19] or photonic local density of state can be gained.[20] Moreover, ET can be combined with holographic techniques to retrieve phase information and quantify electric and magnetic fields in 3D.[21,22]

In electron tomography, 3D information is obtained by acquiring a series of several 2D projection images at different tilt angles. These projection images are then aligned and serve as an input for a reconstruction algorithm to retrieve the 3D morphology and interior structure of the object. To be suitable for reconstruction, the projection images need to fulfill the so-called "projection requirement". This requirement states that the recorded intensities need to represent a sum or integral of a monotonic function of a property, for example, thickness, of the structure.[7] For an optimal reconstruction, the ideal tilt range should be ±90° with a small tilt increment. In contrast to X-ray tomography, where generally a full tilt range of 360° can be achieved, transmission electron microscopes have a restricted physical space between the pole pieces of the objective lens, which limits the tilt range. By using dedicated tomography holders, a typical tilt range of ±75°−80° can be achieved, and the typical tilt increment lies between 1 and 3°. The missing information, which cannot be sampled due to the restriction in tilt range, is typically referred to as the "missing wedge".

Despite the incredible wealth of information that can be gained from ET, the method has one major disadvantage: it is inherently slow. Whether a tilt series is acquired manually or software-automated, several subsequent steps per tilt angle are necessary. Indeed, after tilting the sample to a specific angle, the object of interest needs to be tracked and brought back into the field of view and should be refocused. During conventional ET, these steps need to be repeated ∼50−150 times, where the exact number depends on the chosen tilt range and tilt increment. Hence, acquiring a tomography series typically takes several tens of minutes up to more than 1 h. When combined with

spectroscopic techniques, additional data need to be taken at every tilt angle, which increases the acquisition time to several hours. Consequently, conventional electron tomography is not suitable to obtain a lot of statistics, image beam-sensitive materials, or capture time-resolved processes. Although the ultrafast laser-induced motion of a carbon nanotube has been captured in 3D by using laser-triggered electron pulses,[23] this technique requires repeated acquisition of several tilt series at different time delays and is therefore only suited for reversible processes. The quest for fast ET, which can capture irreversible NP transformations in 3D, is thus a logical next challenge in the field of ET. In this Perspective, we will highlight the recent initial developments in fast ET, with a focus on its necessity for material science, as well as discuss possible strategies to further increase the acquisition speed.

■ RESULTS AND DISCUSSION

Approaches to Fast Electron Tomography. In principle, the acquisition of a tomography series can be performed either in bright-field TEM (BF-TEM) or scanning TEM (STEM) mode. For the former, a parallel beam is used for illumination, and elastically scattered electrons contribute to the image formation. The resulting image can be visualized by a variety of modern cameras such as charge-coupled devices (CCD) or direct electron detectors. For STEM the electron beam is focused into a small probe, and the signal is detected as the amount of electrons scattered to a detector. As the name suggests, the illuminating electron beam in the STEM mode is scanned across the sample, and the signal is built up pixel by pixel. The detection of scattered electrons, which interacted with the sample, is most often performed by using annular detectors. Note that fast ET in diffraction mode has also been achieved.[24]

Concerning (fast) electron tomography, two main differences between TEM and STEM need to be taken into account. First, because of the scanning nature of STEM, it is inherently slower than TEM, where the whole illuminated area is read out at once. Hence, with modern TEM detectors such as sensitive direct electron detectors, good signal-to-noise ratio (SNR) BF-TEM images can be acquired with even more than 1000 frames per second.[25] On the contrary, the acquisition of a single high-quality STEM image generally takes a few seconds, but frame times of 1 s have been shown to result in sufficient SNRs for tomographic reconstructions of inorganic crystals with high scattering.[26] Second, TEM images of crystalline materials contain a significant contribution of so-called diffraction contrast, due to Bragg scattering. Bragg scattered electrons are scattered to small angles, which are collected in BF-TEM. Such diffraction contrast does not fulfill the projection requirement for electron tomography and significantly influences the reliability of reconstructions.[7] Thus, BF-TEM tomography possesses serious limitations for the 3D characterization of crystalline materials. By increasing the amount of electrons that underwent Rutherford scattering, for example, by only collecting electrons that are scattered to high angles (~2−3 times the probe convergence angle[11]), diffraction contrast becomes negligible. In STEM mode, this is typically done by the use of a high-angle annular dark-field (HAADF) detector.

In the next sections, we will discuss different strategies to accelerate the acquisition of a tomography tilt series.

Undersampling. Initial approaches to speed up the acquisition of a tomography series evolved around under-sampling of input data. This can be done either by reducing the amount of projection images (tilt undersampling) or by acquiring faster images with a low signal-to-noise ratio. In STEM, the latter can be achieved either by scanning fewer pixels per projection image or by scanning them fast (intensity undersampling).[27] Both approaches, tilt and intensity under-sampling, are also beneficial with respect to beam damage. It has recently been shown that, for the same applied electron dose, intensity undersampling, by using a lower beam current or scanning faster, yields better reconstruction results than tilt undersampling or scanning fewer pixels per image.[27] It resulted in a shape error of only 1%, even for low-dose cases.

Tilt undersampling is a straightforward approach to reduce the acquisition time of a tomography series. However, the reduction of projection images severely lowers the quality of the reconstruction and might even completely hamper interpreta-tion of the data.[7] Bladt et al. showed that, by training a neural network on a large variety of NPs and making use of an efficient reconstruction algorithm, the number of projection images could be reduced by a factor of 15 without lowering the quality of the reconstruction.[28] This approach enabled high-throughput tomography and statistical 3D analysis.

While undersampling approaches are promising in lowering beam damage and allowing for high-throughput 3D statistics on similar NPs, they have disadvantages when it comes to fast ET. Although making use of neural networks can significantly increase the acquisition time, as fewer projection images are needed, training a neural network requires time. In the case of the work of Bladt et al. full conventional tilt series of NPs from the studied sample were required for training the neural network. Moreover, the training phase needs to be repeated for different sample types. Hence, this approach is very valuable for high-throughput measurements on the same NP sample but is less suited for studying many different sample types or a transforming NP upon external stimuli. In the case of intensity undersampling, the acquisition of each single frame (in STEM) can be increased, but this approach does not accelerate the more time-consuming steps of tilting, tracking, and refocusing at each tilt angle. Consequently, although both undersampling approaches offer solutions for specific problems like beam damage and high throughput, they are not universal solutions. Hence, the entire process of the tomography acquisition needs to be sped up. Emerging simultaneous effort from life sciences and material sciences to lower the acquisition time of a tomography series, especially over the last two to three years, shows the importance of such a fast acquisition for both fields.[24−26,29−33]

Fast Acquisition. Currently, two main approaches have been pursued for fast tomography, in TEM as well as STEM mode: continuous fast ET (CFET) and incremental fast ET (IFET). In CFET, the holder is tilted uninterruptedly from the starting to the finish tilt angle, while simultaneously acquiring a fast image sequence. The possible tilting speed is in principle only limited by the rotation speed of the microscope stage goniometer, and the acquisition of a BF-TEM CFET series with a tilt range of 100° has been demonstrated in less than 4 s when using a direct electron detector.[25] In IFET, the sample is rapidly tilted between consecutive tilting angles, allowing for a predefined relaxation time per angle, while continuously acquiring projection images. The acquisition time depends on the chosen parameters such as relaxation time and tilt increment, and it has been shown to be of the order of a few minutes for TEM and STEM imaging.[24,30−34] An overview of the achieved acquisition times for various experiments reported in the literature is summarized in Table 1.

Table 1. Achieved Acquisition Times and Tilt Ranges for Fast Electron Tomography in Different Modes

reference	mode	tilt range (deg)	acquisition time (s)
Gemmi et al.[24]	TEM (diffraction) CFET	67–92	240–330
Migunov et al.[25]	BF-TEM CFET	100	3.5
Vanrompay et al.[26]	HAADF-STEM CFET	148	~360
Roiban et al.[29]	BF-TEM CFET	116	226
Chreifi et al.[30]	BF-TEM CFET/IFET	102 (CFET) 102–120 (IFET)	12–126 (CFET) 89–190 (IFET)
Koneti et al.[31]	BF-TEM CFET/IFET	136–143 (CFET) 100–140 (IFET)	6–240 (CFET) 140–200 (IFET)
Eisenstein et al.[32]	BF-TEM IFET	120	91–185
Hata et al.[33]	BF-TEM CFET	80	114
Skorikov et al.[34]	HAADF-STEM CFET	150	~360
Epicier et al.[52]	BF-TEM CFET	144	162
Albrecht et al.[54]	HAADF-STEM CFET	150	~360
Park et al.[38]	BF-TEM NP rotation in liquid		23–31

Both acquisition schemes have advantages and limitations. In both cases, lateral and vertical movement of the stage while tilting requires repositioning the object of interest in the field of view (x,y) and refocusing (z). Whereas specimen movements parallel to the tilt axis were found to be negligible, shifts perpendicular to the tilt axis are on the order of several hundreds of nanometers over a full tilt range.[30,32] Changes in z height and hence defocus are on the order of microns.[32] In both cases, for lateral and vertical shifts, the movements worsen for higher tilt angles. Although these shifts can be partially compensated for by estimating the movement through precalibration of the stage at the specific stage position,[35,36] they severely limit the possible image magnification and/or tilt range, which increases the missing wedge artifact.[25,31] Hence, for best image quality, it is necessary to manually correct for stage movements while acquiring the fast tomography series. This generally increases the acquisition time in TEM and STEM mode for both acquisition schemes to above 1 min as seen in Table 1. Moreover, additional overhead due to the preparation of the tilt series and possible software dead time after saving the acquired image series also need to be taken into account and can be on the order of minutes.[30,32]

For CFET, an additional problem occurs. Because of the continuous mechanical movement of the goniometer, blurring artifacts in TEM mode and scanning distortions seen as streaking artifacts in STEM mode occur.[26,31] Moreover, as the specimen is tilted while an image is acquired in the STEM mode, a careful ratio between frame time and tilting speed needs to be found to avoid that the tilt angle changes significantly in one frame.[26] These effects lower the quality of the reconstruction. For TEM acquisition it has been shown that a tilt of less than 2° per frame reduces blurring artifacts sufficiently.[31] For STEM, recent results indicate that the deteriorating effect of streaking artifacts in STEM becomes significant, when the size of the studied features is comparable to the amplitude of the distortions, which is true for NPs with small details such as nanostars with sharp tips. These artifacts can be circumvented by using the IFET approach, which results in a better reconstruction quality but makes it harder to track the object of interest.[37] To summarize, IFET is the optimal choice for obtaining a high-quality tilt series at intermediate acquisition times. CFET is currently more suitable for BF-TEM, and in this manner tomography acquisition times on the order of seconds can be achieved. We believe that future research can significantly improve the compatibility of CFET with HAADF-STEM as laid out in the Outlook section.

Note that, for experiments in liquid environments, fast tomographic acquisition can be achieved by making use of the rotation of NPs in liquid without having to tilt the holder. In this manner, near-atomic resolution in 3D has recently been achieved by acquiring a movie of a single rotating Pt NP in liquid in ~30 s.[38] In a follow-up work, the authors developed an elaborate reconstruction method by tracking individual particles over time and correcting for particle motion and background.[39] This methodology enabled the authors to obtain the 3D atomic positions of several Pt NPs and to determine structural differences between them such as internal defects and lattice strain. Although the technique is limited to liquid environments, it is an innovative approach, which is fast and can fully circumvent missing wedge artifacts.

Application to Material Science. Although several technical obstacles still need to be overcome, pioneering work has demonstrated that fast ET is already capable of delivering valuable insight in material science. Specifically, the 3D characterization of beam-sensitive materials and dynamic processes becomes feasible, as we will exemplify below.

Beam-Sensitive Materials. Imaging materials, which change upon illumination with the electron beam, is already challenging in 2D, yet alone in 3D.[40] Organic matter is almost always highly beam-sensitive, but inorganic crystals such as perovskites or zeolites are known to easily degrade under the electron beam as well.[41,42] Different damage mechanisms are relevant for different materials and have been reviewed elsewhere.[40] One way of reducing beam-induced damage is cooling the specimen below 100 K, as it slows down atomic diffusion and consequently chemical reactions.[40] Although cryo-ET has been successfully used to predominantly visualize organic biological matter in 3D,[43,44] it is less used for inorganic materials and NPs, as it is a difficult technique and limited in resolution. Fast ET is a promising tool to reduce the interaction time between the specimen and the electron beam and hence lower the dose below the damage threshold.

Koneti and co-workers succeeded in imaging magnetotactic bacteria in 3D in noncryo conditions by making use of BF-IFET with an acquisition time of 140 s and a tilt range of 100°.[31] This acquisition was possible because, by accelerating the acquisition speed of the tomography series, the electron dose could be kept below the damage threshold. In the same publication, the authors furthermore demonstrate a successful BF-IFET experiment on a polymer nanocomposite. The corresponding results are shown in Figure 1a−e. The investigated polymer complex was made of a soft latex reinforced with Mg_3AlCO_3 layered
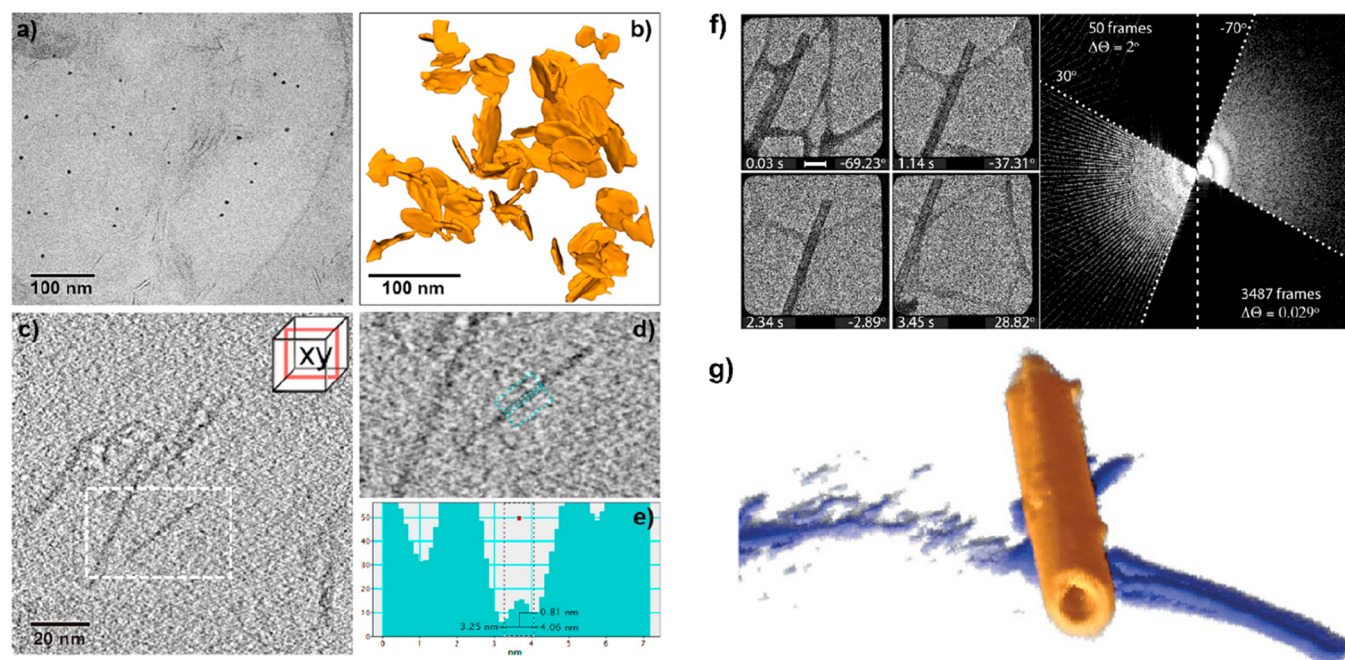
Figure 1. Examples of beam-sensitive materials that could only be studied by fast ET and would be destroyed by conventional ET. The left example depicts fast BF-TEM results on a polymer nanocomposite. (a) BF-TEM image of the composite, (b) reconstructed Mg_3AlCO_3 nanoplatelets embedded in the polymer matrix, (c) slice through the reconstruction and its enlargement, (d, e) intensity profile across the marked platelet indicating a resolution of 0.8 nm. Reprinted with permission from ref 31. Copyright 2019 Elsevier. The right example shows the results of CFET experiments in BF-TEM mode on a $(LaCeS)_{1.2}CrS_2$ nanotube performed in 3.5 s. (f) Examples of projection images at different tilt angles (left) and sampling in Fourier space (right). (g) 3D visualization of the reconstructed nanotube using the DART algorithm. Reprinted with permission from ref 25. Copyright 2015 Springer Nature.

double hydroxide nanoplatelets. After defining a critical dose by preliminary irradiation tests, the authors acquired a BF-IFET series over a tilt range of 140° in 200 s. Figure 1a shows the projection image at 0° tilt, where the gray lines are the platelets and black dots are Au NPs used for alignment of the series. The segmented reconstruction of the nanoplatelets and cross-section through the volume are shown in Figure 1b,c, respectively. Figure 1d,e demonstrates the expected spacing of 0.8 nm for these platelets. Since the authors could measure that spacing from the reconstruction, it shows that they had a resolution better than 1 nm^3. Migunov et al. performed a CFET experiment in BF-TEM in only 3.5 s for a tilt range of 100° on an inorganic nanotube (Figure 1f,g).[25] Although the tilt range was limited, because for higher tilt angles the nanotube went out of the field of view, the authors demonstrate that the use of the discrete algebraic reconstruction technique (DART) could reduce the missing wedge artifacts compared to a more conventional simultaneous iterative reconstruction technique (SIRT) algorithm.

Dynamic Processes. In situ studies in the electron microscope have become a powerful tool to understand nanoscale and atomic processes upon external stimuli such as heat, gas or liquid environment, magnetic fields, or mechanical stress.[45] These studies have either been performed with dedicated microscopes, such as an environmental transmission electron microscope (ETEM),[46,47] or dedicated holders making use of microelectromechanical systems (MEMS) devices.[48−50] Despite the technical advances in ETEMs and MEMS devices, in situ studies have only recently been performed in 3D, coupled to the development of fast tomography. The reason is that dynamic processes, which can be observed in situ inside the electron microscope, are simply too fast to be captured by conventional

ET. In principle, an ET analysis could be performed post mortem, meaning that the ET acquisition is performed after different stages of an ex situ experiment. However, this approach prohibits the direct visualization of ongoing transformations and, when using conventional ET, limits the amount of data that can be taken due to the long acquisition times. Thus, the natural way forward is to combine in situ and operando studies with fast ET. It should be mentioned that (fast) ET has been employed for studying material transformations upon exerting mechanical stress, which has recently been reviewed elsewhere.[51] Here, we focus on the dynamic processes of nanoparticles.

One of the first fast operando ET experiments of nanocatalysts has been performed by Roiban and co-workers.[29] The authors studied the evolution of Ag NPs in hollow silicalite-1 zeolites under oxygen environment at different temperatures (Figure 2a−c). For that, they used an ETEM microscope with a Gatan heating holder. CFET data sets were acquired within ∼2 min each at 20 °C in high vacuum (Figure 2a) and at 280 and 450 °C at 1.8 mbar of O_2 (Figure 2b,c). In these experiments, the tilt range was limited to 67°. Despite the consequent large missing wedge, the authors could perform a statistical analysis of the Ag NPs. They found that the total Ag volume remained constant but that the particle size increased from 6.7 nm at 20 °C to 7.6 nm at 280 °C with a decrease in particle number from 56 to 41, which the authors addressed to Ostwald ripening. At 450 °C, the numbers of NPs dropped to 15, and most of them moved outside the silica cages. The authors concluded that silver gets oxidized once the zeolite pores are free of organic material, and the resulting silver oxide decomposes and vaporizes leaving the zeolite pores, and metallic NPs are subsequently reformed on the support grid. These findings have direct relevance for the preparation protocol of Ag-loaded hollow zeolites.
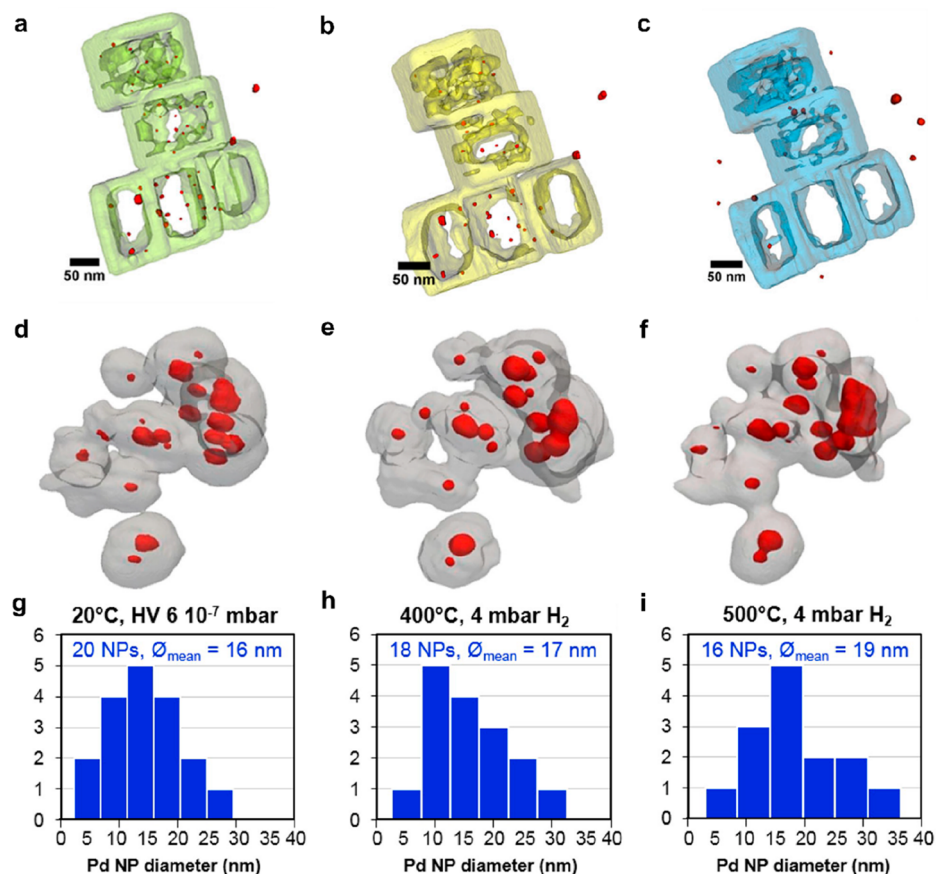
Figure 2. In situ heating of Ag NPs in hollow silicalite-1 zeolites in an O_2 environment and Pd@SiO$_2$ aggregates in a H_2 atmosphere. 3D visualizations of the tomographic reconstructions of Ag NPs (red) in hollow silicalite-1 zeolites are shown (a) in high vacuum at 20 °C, (b) at 280 °C, and (c) at 450 °C under 1.8 mbar of O_2. Adapted with permission from ref 29. Copyright 2017 John Wiley and Sons. 3D visualizations of the tomographic reconstructions of the Pd@SiO$_2$ aggregates are shown (d) in high vacuum at 20 °C, (e) at 400 °C, and (f) at 500 °C under 4 mbar of H_2, where the Pd NPs are depicted in red and the SiO$_2$ shell is in gray. The corresponding CFET BF-TEM series were each acquired in 6−9 s. (d−f) Histograms of the size distributions of the Pd NPs extracted from the reconstructions. Adapted with permission from ref 31. Copyright 2019 Elsevier.

In a follow-up study, the same group imaged the 3D evolution of Pd/alumina agglomerates upon calcination in 2.6 mbar of oxygen at 350 °C in 162 s. After calcination, the density of Pd NPs in the alumina increased without a significant decrease in distance between neighboring particles.[52] The same group also visualized sintering of silica-coated Pd NPs upon heating under H_2 atmosphere in the ETEM.[31] By using a dedicated DENSsolutions heating ET holder, they could lower the acquisition time of the BF-CFET series to 6−9 s with a tilt range of 143°. The results at 20 °C in high vacuum and at 400 and 500 °C in 4 mbar of H_2 are shown in Figure 2. Because of the H_2 environment, the SNR of the projection images was low, and the authors used a homemade reconstruction algorithm to compensate for it.[53] As can be seen in Figure 2d−f, upon heating in H_2, Pd NPs merged together. Statistical analysis (Figure 2g−i) revealed that the average NP size increased and the number of NPs decreased from 20 to 16, evidencing coalescence. Both initial work on sintering of Ag and Pd NPs in matrices shows the importance of combining fast ET and in situ processes. First, the beam-sensitive silicates would have been destroyed by conventional ET. Second, the volume, density, and location analysis of the metal NPs would not have been possible when performed in 2D or ex situ.

While the speed achieved in the work related to Figure 2 is remarkable, it needs to be kept in mind that BF-TEM ET suffers from diffraction contrast and is not readily applicable to all crystalline samples. As a consequence, the Electron Microscopy for Materials Science group at the University of Antwerp committed to increasing the speed of HAADF-STEM ET, allowing for detailed in situ visualizations of crystalline NPs with high resolution.[26,34,54] In a first study, the group determined the heat-induced morphological transformation of highly anisotropic Au nanostars (NSs) as shown in Figure 3.[26] For that, CFET in HAADF-STEM mode was performed by continuously rotating a MEMS-based heating tomography holder from DENSsolutions while manually refocusing and repositioning. In that manner, an ET series could be acquired over a tilt range of 148° in 6 min, which is approximately an order of magnitude faster than the acquisition of a conventional HAADF-STEM ET series. Moreover, a relatively high magnification (pixel size of 386 pm) could be used resulting in high-quality reconstructions with a negligible difference to a conventional series. Nine 3D data sets were acquired at three different temperatures to monitor the heat-induced changes of single NSs over a course of 1200 s of heating. During the acquisition of a CFET series, the specimen was quenched to 25 °C to avoid changes of the NPs during the acquisition. However, in this manner, it is also possible to sample any time step of the transformation. The morphological changes were then analyzed by comparing the different reconstructions to each other (Figure 3a−i). With this methodology, it could directly be visualized that volume redistributed from areas of high curvature (tips) to areas of
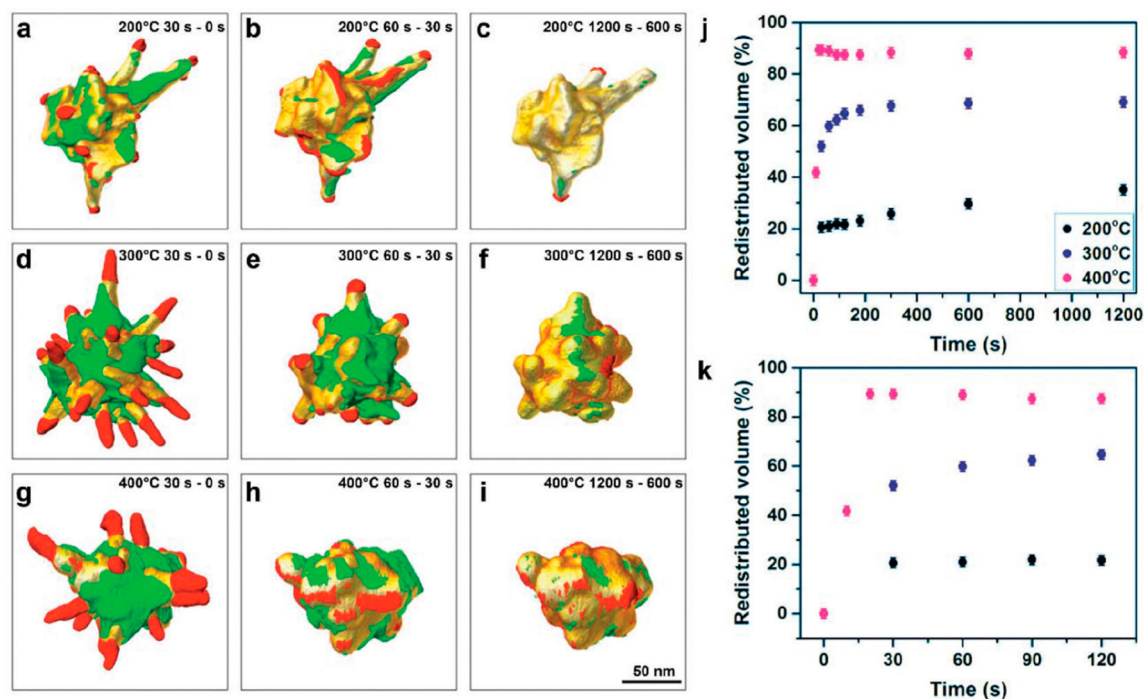
Figure 3. In situ heating of Au nanostars (NS) making use of HAADF-STEM CFET. (a–i) Visualizations of the morphological changes during two successive heating steps, where volume increments and volume reductions are depicted in green and red, respectively. The order of subtraction is indicated in each panel, together with the temperature of heating. (j) Total amount of redistributed volume normalized to the volume of the branches in the initial NS, as a function of time for 200 °C (black dots), 300 °C (blue dots), and 400 °C (magenta dots). (k) Detailed view of the volume redistribution occurring during the first 2 min. Reprinted with permission from ref 26. Copyright 2018 Royal Society of Chemistry.
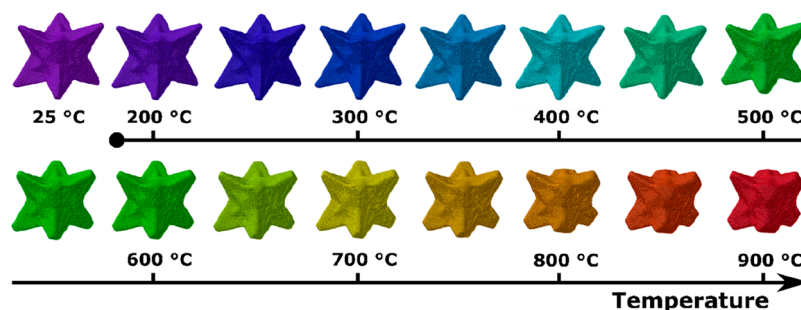

Figure 4. 3D visualization of the same Au/Pd octopod before (25 °C) heating and after heating for 5 min at intermediate temperatures between 200 and 900 °C. Each tomographic tilt series was acquired in HAADF-STEM mode over a tilt range of 150° in ~360 s. Reprinted with permission from ref 54. Copyright 2019 American Chemical Society.

low curvature (side). Furthermore, by quantifying the redistributed volume, it could be measured that most deformation happened in the first minute of heating with stronger deformations at higher temperatures (Figure 3j,k). Moreover, the evolution of curvature of the NSs could be quantified as a function of heating time and temperature, which is directly relevant for their usage in plasmonic applications.

In a follow-up work, the HAADF-STEM CFET methodology was used to understand the heat-induced reshaping of AuPd octopods.[54] Sixteen CFET HAADF-STEM series of the same AuPd octopod were acquired between 25 and 900 °C (Figure 4), each with a tilt range of 150° and acquisition time of ~6 min. It was observed that, due to just a low amount of Pd, the thermal stability of octopods could be drastically increased. By quantifying the morphological changes, it became obvious that no reshaping occurred up to 450 °C and that, up to 750 °C, only 4% of the volume redistributed. On the contrary, pure Au octopods already reshaped at 200 °C. Similar to the Au NSs, the

octopods deformed by volume redistribution from the tips to the sides of the particle. Because of the remarkable stability of the AuPd octopods, the particles maintained their plasmonic properties up to 600 °C, which was determined by EELS. The observations reveal that AuPd octopods are good candidates for high-temperature plasmonic applications.

One major advantage of STEM over TEM lies in the so-called Z contrast, which can give information about the chemical composition of the material as different elements scatter electrons to different angles. In combination with CFET, Skorikov et al. made use of the Z contrast to study alloying in single Au@Ag@SiO$_2$ NPs of varying shapes as presented in Figure 5a.[34] Hereby, the mesoporous silica shell prevented morphological changes of the bimetallic NPs. The NPs were heated to 450 °C inducing alloying. The reaction was quenched at several time steps, and the CFET series were acquired with ~6 min of acquisition time each. Slices through the reconstructions are shown in Figure 5b–d. The composition in the
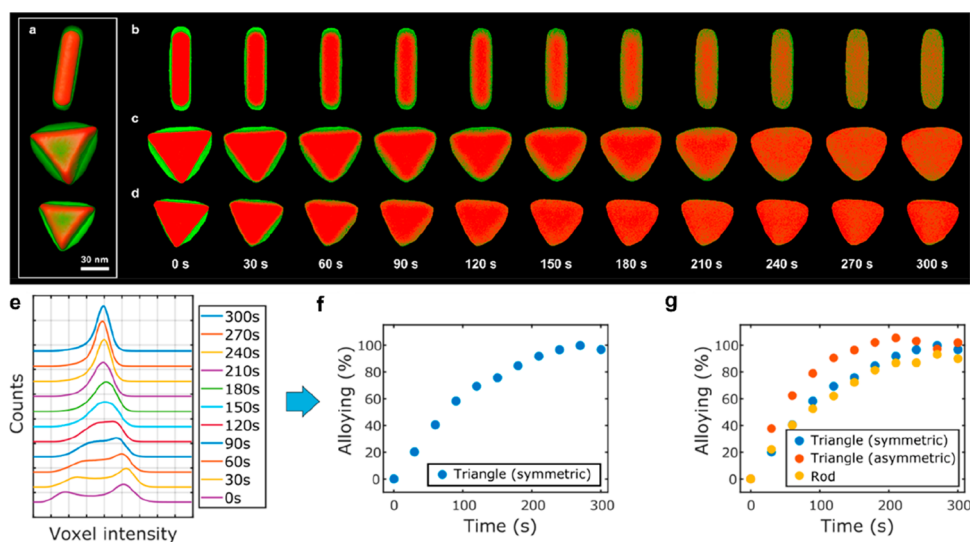
Figure 5. In situ heating experiment of Au@Ag@SiO₂ NPs of varying shape, which were measured by HAADF-STEM CFET. (a) Visualizations of 3D reconstructions for the varying NP shapes. (b−d) Slices through the 3D reconstructions of elemental distributions inside the nanorod, the symmetric, and the asymmetric nanotriangles, respectively, at different stages of alloying at 450 °C. By making use of the Z contrast in HAADF-STEM, the elemental distributions can be visualized. Here, red and green depict Au and Ag, respectively. (e) Evolution of the histogram of voxel intensities in the reconstruction of the symmetric nanotriangle during alloying. (f) Progress of alloying for the symmetric nanotriangle during heating at 450 °C, estimated from the spread of histograms of voxel intensities in the reconstruction. (g) Comparison of the alloying dynamics for the nanorod, the symmetric, and the asymmetric nanotriangles. Adapted with permission from ref 34. Copyright 2019 American Chemical Society.

reconstructions was quantified based on the changing voxel intensity histograms in the particles upon alloying (Figure 5e). This quantification allowed to determine the degree of alloying as a function of time (Figure 5f,g) for the different particles. By fitting the experimental results to diffusion simulations, diffusion coefficients could then be extracted on a single NP level. This approach can be used for a variety of bicomponent systems and opens the pathway to study elemental redistribution dynamics for a single NP level as a function of composition, morphology, and size.

The last three examples demonstrate that, although fast STEM ET is still slower than fast BF-TEM ET, it allows to study in situ processes on (single-)crystalline NPs and makes it possible to track elemental changes due to Z contrast. Ultimately, the method chosen for a specific experiment is dictated by the material. For noncrystalline materials, BF-TEM already offers fast ET acquisition on the order of seconds. To avoid diffraction contrast, HAADF-STEM tomography is needed for crystalline samples.

■ CONCLUSIONS AND OUTLOOK

The initial examples presented in this Perspective demonstrate the value of fast tomography for the material science community. Although still at its beginning, fast tomography data sets have already been acquired at very fast speeds on the order of seconds (BF-TEM) and allowed for chemical contrast while excluding diffraction contrast (HAADF-STEM). Yet, ideally both worlds should be combined in one approach. One path is to eliminate diffraction contrast in BF-TEM. Although experimental approaches exist to remove unwanted diffraction contrast in BF-TEM,[55−58] most of them are rather complicated and time-consuming, as they, for example, require additional data such as several images at different defocus values per angle.[55] A relatively straightforward approach without an increase in additional acquisition time is to make use of carefully designed apertures to exclude those electrons that are responsible for diffraction

contrast in BF-TEM.[59] This technique, commonly referred to as annular dark-field TEM, has the additional advantage that lower exposure times than for HAADF-STEM are needed for good image quality.[59] An alternative path is to further enhance the acquisition speed of HAADF-STEM tomography. For that several obstacles need to be overcome.

To make fast ET in HAADF-STEM mode faster, several possibilities exist, as it can be combined with the original undersampling ideas. Currently, the results for fast HAADF-STEM ET were obtained with a 1 s frame time. However, the results of the above-discussed undersampling study suggest that much faster scanning times are possible by intensity undersampling, which then allows for a faster tilting speed.[27] For the IFET approach, tilt undersampling can be compensated by advanced analysis as already achieved by training neural networks.[28] Although this approach is especially useful for a high-throughput 3D analysis of the same NP type, novel neural network techniques might be able to extend that to changing NPs in in situ studies. For that, the ET community can take advantage of effort in other tomography domains. Specifically, for magnetic resonance imaging and X-ray tomography, several deep neural networks have been designed to reliably reconstruct tomograms from limited data.[60−63] For sure, neural networks can also be utilized for improving the image quality of noisy and possibly distorted projection images, which are unavoidable in fast acquisition schemes.[64,65] Such image restorations have already led to a breakthrough in atomic resolution tomography and are expected to have a similar impact for fast ET.[13,66]

Deep learning approaches will also be valuable to accelerate the acquisition of spectroscopic tomography. Combining fast HAADF-STEM tomography with EDXS or EELS will already increase the acquisition speed, compared to a conventional acquisition. In addition, by making use of neural networks to denoise the spectroscopic data, the acquisition time of each EDXS or EELS map can be significantly lowered. In parallel, the SNR ratio can be enhanced by advanced low-background

substrates such as graphene. Although an acquisition of only a few seconds will most likely not be achievable, in this manner current acquisition times of several hours can still be decreased to possibly below 1 h.

The work on fast ET so far shows that a faster acquisition with noisier images and a larger missing wedge goes along with the development of advanced reconstruction algorithms.[53,67] Next to improving the quality of the reconstruction, dynamic processes could be implemented in the reconstruction process itself.[68−70] In that way, a tilt series of a changing object could be reliably reconstructed, and the acquisition does not need to happen in a stop-and-go fashion. This is not an easy task and might simply not work for complex irreversible processes. However, for movements or reversible processes that can be estimated to some extent, such as NPs moving in liquid, such reconstruction algorithms will boost the performance of in situ 3D analysis.

When the sample is tilted faster than an image can be acquired, rotation blurring occurs in BF-TEM, and in HAADF-STEM the tilting angle might change per scanned line. In BF-TEM that can be overcome by fast direct electron detectors, which acquire images faster than the holder can be tilted in current goniometers.[25,31] In STEM mode this problem can be overcome, when the tilt increment per acquired frame is known, by reconstructing the tomogram line-by-line rather than frame-by-frame. With the considerations so far, there is in principle no reason why STEM cannot reach similar time scales as those of TEM tomography, albeit at the cost of more advanced data processing.

The ultimate current limitation to achieve a fast ET acquisition with very fast speed, high tilt range, and resolution at the same time are the mechanical instabilities of the microscope goniometers, which lead to lateral and vertical movements while tilting. Future improvements in microscope development on the manufacturer side and advanced on-the-fly or precalibrated drift and defocus correction will be necessary. Mechanical-free rotation of the specimen might be an interesting alternative, which is already possible in liquid environments as discussed above.

An exciting endeavor is to combine fast tomography with automated parallel reconstruction and analysis to perform live in situ and operando tomography. Such on-the-fly reconstruction has just been realized allowing for real-time 3D feedback and on-the-fly quantification, paving the path for high-throughput and routine NP 3D characterization.[71] The combined effort in fast tomography acquisition and advanced reconstruction algorithms will most definitely lead to new scientific breakthroughs in material science. The main areas that benefit from that development will be beam-sensitive materials, such as perovskites and zeolites, as well as in situ and operando microscopy. Here, fast ET will improve understanding of catalytic and assembly processes as well as NP and phase transformations upon stimuli and growth of NPs in solution.

■ AUTHOR INFORMATION

Corresponding Author

Sara Bals − EMAT and NANOlab Center of Excellence, University of Antwerp, B-2020 Antwerp, Belgium; ● orcid.org/0000-0002-4249-8017; Email: Sara.Bals@ uantwerpen.be

Author
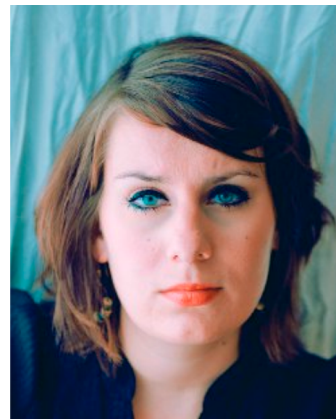
Wiebke Albrecht − EMAT and NANOlab Center of Excellence, University of Antwerp, B-2020 Antwerp, Belgium

Complete contact information is available at:
https://pubs.acs.org/10.1021/acs.jpcc.0c08939

Notes

The authors declare no competing financial interest.

Biographies

Julia Trauer

Dr. Wiebke Albrecht received her PhD in Physics from Utrecht University in 2017 and works currently as a postdoctoral researcher at the University of Antwerp. Her research is focussed on heat and laser-induced transformations of anisotropic metal and semiconductor nanoparticles. Her current research interests are also directed at the correlation of optical and structural properties of nanoparticles. In 2018, she was awarded with a Marie Skłodowska-Curie Actions Individual fellowship to pursue that correlation at the single-nanoparticle level by combining optical and transmission electron microscopy techniques.
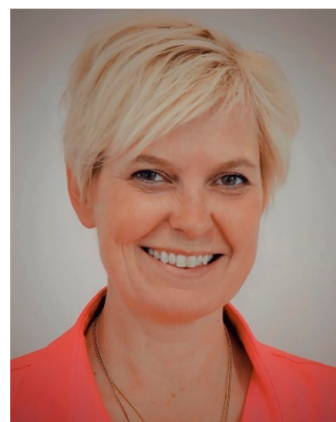
Liesbet Laurens

Prof. dr. Sara Bals received her PhD in Physics at the University of Antwerp in 2003 and is a professor at the same university since 2007. Since 2015, she is the spokesperson of the electron microscopy group EMAT. She did postdoctoral work at the National Center for Electron Microscopy in Berkeley, California. During this period, she initiated her current research line on electron tomography applied to functional nanomaterials. In 2013, she received an ERC Starting Grant on the 3D characterization of nanostructures (structure, composition, and bonding) at the atomic scale (COLOURATOM). In 2016, she became "Laureate of the Academy for Natural Sciences" awarded by the Royal Flemish Academy of Belgium for Science and the Arts. In 2017, she was

■ REFERENCES

(1) DeSantis, C. J.; Skrabalak, S. E. Manipulating the Optical Properties of Symmetrically Branched Au/Pd Nanocrystals through Interior Design. *Chem. Commun.* **2014**, *50*, 5367−5369.

(2) Li, N.; Zhao, P.; Astruc, D. Anisotropic Gold Nanoparticles: Synthesis, Properties, Applications, and Toxicity. *Angew. Chem., Int. Ed.* **2014**, *53*, 1756−1789.

(3) González-Rubio, G.; Mosquera, J.; Kumar, V.; Pedrazo-Tardajos, A.; Llombart, P.; Solís, D. M.; Lobato, I.; Noya, E. G.; Guerrero-Martínez, A.; Taboada, J. M.; et al. Micelle-Directed Chiral Seeded Growth on Anisotropic Gold Nanocrystals. *Science* **2020**, *368*, 1472−1477.

(4) Cortie, M. B.; McDonagh, A. M. Synthesis and Optical Properties of Hybrid and Alloy Plasmonic Nanoparticles. *Chem. Rev.* **2011**, *111*, 3713−3735.

(5) Ha, M.; Kim, J. H.; You, M.; Li, Q.; Fan, C.; Nam, J. M. Multicomponent Plasmonic Nanoparticles: From Heterostructured Nanoparticles to Colloidal Composite Nanostructures. *Chem. Rev.* **2019**, *119*, 12208−12278.

(6) Van Tendeloo, G.; Bals, S.; Van Aert, S.; Verbeeck, J.; Van Dyck, D. Advanced Electron Microscopy for Advanced Materials. *Adv. Mater.* **2012**, *24*, 5655−5675.

(7) Midgley, P. A.; Weyland, M. 3D Electron Microscopy in the Physical Sciences: The Development of Z-Contrast and EFTEM Tomography. *Ultramicroscopy* **2003**, *96*, 413−431.

(8) Midgley, P. A.; Dunin-Borkowski, R. E. Electron Tomography and Holography in Materials Science. *Nat. Mater.* **2009**, *8*, 271−280.

(9) Ersen, O.; Florea, I.; Hirlimann, C.; Pham-Huu, C. Exploring Nanomaterials with 3D Electron Microscopy. *Mater. Today* **2015**, *18*, 395−408.

(10) Zhang, Q.; Hernandez, T.; Smith, K. W.; Hosseini Jebeli, S. A.; Dai, A. X.; Warning, L.; Baiyasi, R.; McCarthy, L. A.; Guo, H.; Chen, D. H.; et al. Unraveling the Origin of Chirality from Plasmonic Nanoparticle-Protein Complexes. *Science* **2019**, *365*, 1475−1478.

(11) Winckelmans, N.; Altantzis, T.; Grzelczak, M.; Sánchez-Iglesias, A.; Liz-Marzán, L. M.; Bals, S. Multimode Electron Tomography as a Tool to Characterize the Internal Structure and Morphology of Gold Nanoparticles. *J. Phys. Chem. C* **2018**, *122*, 13522−13528.

(12) Smith, J. D.; Bladt, E.; Burkhart, J. A. C.; Winckelmans, N.; Koczkur, K. M.; Ashberry, H. M.; Bals, S.; Skrabalak, S. E. Defect-Directed Growth of Symmetrically Branched Metal Nanocrystals. *Angew. Chem., Int. Ed.* **2020**, *59*, 943−950.

(13) Milagres de Oliveira, T.; Albrecht, W.; González-Rubio, G.; Altantzis, T.; Lobato Hoyos, I. P.; Béché, A.; Van Aert, S.; Guerrero-Martínez, A.; Liz-Marzán, L. M.; Bals, S. 3D Characterization of Gold Nanorods after Welding under Femtosecond Laser Irradiation. *ACS Nano* **2020**, *14*, 12558−12570.

(14) Goris, B.; Bals, S.; Van den Broek, W.; Carbó-Argibay, E.; Gómez-Graña, S.; Liz-Marzán, L. M.; Van Tendeloo, G. Atomic-Scale Determination of Surface Facets in Gold Nanorods. *Nat. Mater.* **2012**, *11*, 930−935.

(15) Goris, B.; De Beenhouwer, J.; De Backer, A.; Zanaga, D.; Batenburg, K. J.; Sánchez-Iglesias, A.; Liz-Marzán, L. M.; Van Aert, S.; Bals, S.; Sijbers, J.; et al. Measuring Lattice Strain in Three Dimensions through Electron Microscopy. *Nano Lett.* **2015**, *15*, 6996−7001.

(16) Goris, B.; Polavarapu, L.; Bals, S.; Van Tendeloo, G.; Liz-Marzán, L. M. Monitoring Galvanic Replacement through Three-Dimensional Morphological and Chemical Mapping. *Nano Lett.* **2014**, *14*, 3220−3226.

(17) Zanaga, D.; Altantzis, T.; Polavarapu, L.; Liz-Marzán, L. M.; Freitag, B.; Bals, S. A New Method for Quantitative XEDS Tomography of Complex Heteronanostructures. *Part. Part. Syst. Charact.* **2016**, *33*, 396−403.

(18) Feld, A.; Weimer, A.; Kornowski, A.; Winckelmans, N.; Merkl, J.-P.; Kloust, H.; Zierold, R.; Schmidtke, C.; Schotten, T.; Riedner, M.; et al. Chemistry of Shape-Controlled Iron Oxide Nanocrystal Formation. *ACS Nano* **2019**, *13*, 152−162.

(19) Goris, B.; Meledina, M.; Turner, S.; Zhong, Z.; Batenburg, K. J.; Bals, S. Three Dimensional Mapping of Fe Dopants in Ceria Nanocrystals Using Direct Spectroscopic Electron Tomography. *Ultramicroscopy* **2016**, *171*, 55−62.

(20) Horl, A.; Haberfehlner, G.; Trugler, A.; Schmidt, F. P.; Hohenester, U.; Kothleitner, G. Tomographic Imaging of the Photonic Environment of Plasmonic Nanoparticles. *Nat. Commun.* **2017**, *8*, 37.

(21) Wolf, D.; Biziere, N.; Sturm, S.; Reyes, D.; Wade, T.; Niermann, T.; Krehl, J.; Warot-Fonrose, B.; Büchner, B.; Snoeck, E.; et al. Holographic Vector Field Electron Tomography of Three-Dimensional Nanomagnets. *Commun. Phys.* **2019**, *2*, 87.

(22) Wolf, D.; Lubk, A.; Röder, F.; Lichte, H. Electron Holographic Tomography. *Curr. Opin. Solid State Mater. Sci.* **2013**, *17*, 126−134.

(23) Kwon, O.-H.; Zewail, A. H. 4D Electron Tomography. *Science* **2010**, *328*, 1668−1673.

(24) Gemmi, M.; La Placa, M. G. I.; Galanis, A. S.; Rauch, E. F.; Nicolopoulos, S. Fast Electron Diffraction Tomography. *J. Appl. Crystallogr.* **2015**, *48*, 718−727.

(25) Migunov, V.; Ryll, H.; Zhuge, X.; Simson, M.; Strüder, L.; Batenburg, K. J.; Houben, L.; Dunin-Borkowski, R. E. Rapid Low Dose Electron Tomography Using a Direct Electron Detection Camera. *Sci. Rep.* **2015**, *5*, 14516.

(26) Vanrompay, H.; Bladt, E.; Albrecht, W.; Béché, A.; Zakhozheva, M.; Sánchez-Iglesias, A.; Liz-Marzán, L. M.; Bals, S. 3D Characterization of Heat-Induced Morphological Changes of Au Nanostars by Fast in Situ Electron Tomography. *Nanoscale* **2018**, *10*, 22792−22801.

(27) Vanrompay, H.; Béché, A.; Verbeeck, J.; Bals, S. Experimental Evaluation of Undersampling Schemes for Electron Tomography of Nanoparticles. *Part. Part. Syst. Charact.* **2019**, *36*, 1900096.

(28) Bladt, E.; Pelt, D. M.; Bals, S.; Batenburg, K. J. Electron Tomography Based on Highly Limited Data Using a Neural Network Reconstruction Technique. *Ultramicroscopy* **2015**, *158*, 81−88.

(29) Roiban, L.; Li, S.; Aouine, M.; Tuel, A.; Farrusseng, D.; Epicier, T. Fast 'Operando' Electron Nanotomography. *J. Microsc.* **2018**, *269*, 117−126.

(30) Chreifi, G.; Chen, S.; Metskas, L. A.; Kaplan, M.; Jensen, G. J. Rapid Tilt-Series Acquisition for Electron Cryotomography. *J. Struct. Biol.* **2019**, *205*, 163−169.

(31) Koneti, S.; Roiban, L.; Dalmas, F.; Langlois, C.; Gay, A.-S.; Cabiac, A.; Grenier, T.; Banjak, H.; Maxim, V.; Epicier, T. Fast Electron Tomography: Applications to Beam Sensitive Samples and in Situ TEM or Operando Environmental TEM Studies. *Mater. Charact.* **2019**, *151*, 480−495.

(32) Eisenstein, F.; Danev, R.; Pilhofer, M. Improved Applicability and Robustness of Fast Cryo-Electron Tomography Data Acquisition. *J. Struct. Biol.* **2019**, *208*, 107−114.

(33) Hata, S.; Miyazaki, S.; Gondo, T.; Kawamoto, K.; Horii, N.; Sato, K.; Furukawa, H.; Kudo, H.; Miyazaki, H.; Murayama, M. In-Situ Straining and Time-Resolved Electron Tomography Data Acquisition in a Transmission Electron Microscope. *Microscopy* **2016**, *66*, 143−153.

(34) Skorikov, A.; Albrecht, W.; Bladt, E.; Xie, X.; van der Hoeven, J. E. S.; van Blaaderen, A.; Van Aert, S.; Bals, S. Quantitative 3D Characterization of Elemental Diffusion Dynamics in Individual Ag@ Au Nanoparticles with Different Shapes. *ACS Nano* **2019**, *13*, 13421−13429.

(35) Ziese, U.; Janssen, A. H.; Murk, J.-L.; Geerts, W. J. C.; Van Der Krift, T.; Verkleij, A. J.; Koster, A. J. Automated High-Throughput Electron Tomography by Pre-Calibration of Image Shifts. *J. Microsc.* **2002**, *205*, 187−200.

(36) Mastronarde, D. N. Automated Electron Microscope Tomography Using Robust Prediction of Specimen Movements. *J. Struct. Biol.* **2005**, *152*, 36−51.

(37) Vanrompay, H.; Skorikov, A.; Bladt, E.; Béché, A.; Freitag, B.; Verbeeck, J.; Bals, S. Fast versus Conventional HAADF-STEM Tomography: Advantages and Challenges. *arXiv (Materials Science)*, September 20, 2020, 2009.14512, ver. 1. https://arxiv.org/abs/2009.14512 (accessed October 1, 2020).

(38) Park, J.; Elmlund, H.; Ercius, P.; Yuk, J. M.; Limmer, D. T.; Chen, Q.; Kim, K.; Han, S. H.; Weitz, D. A.; Zettl, A.; et al. 3D Structure of Individual Nanocrystals in Solution by Electron Microscopy. *Science* **2015**, *349*, 290−295.

(39) Kim, B. H.; Heo, J.; Kim, S.; Reboul, C. F.; Chun, H.; Kang, D.; Bae, H.; Hyun, H.; Lim, J.; Lee, H.; et al. Critical Differences in 3D Atomic Structure of Individual Ligand-Protected Nanocrystals in Solution. *Science* **2020**, *368*, 60−67.

(40) Egerton, R. F. Radiation Damage to Organic and Inorganic Specimens in the TEM. *Micron* **2019**, *119*, 72−87.

(41) Sasaki, Y.; Suzuki, T. Formation of Ag Clusters by Electron Beam Irradiation of Ag-Zeolites. *Mater. Trans.* **2009**, *50*, 1050−1053.

(42) Dang, Z.; Shamsi, J.; Palazon, F.; Imran, M.; Akkerman, Q. A.; Park, S.; Bertoni, G.; Prato, M.; Brescia, R.; Manna, L. In Situ Transmission Electron Microscopy Study of Electron Beam-Induced Transformations in Colloidal Cesium Lead Halide Perovskite Nanocrystals. *ACS Nano* **2017**, *11*, 2124−2132.

(43) Oikonomou, C. M.; Jensen, G. J. Cellular Electron Cryotomography: Toward Structural Biology in Situ. *Annu. Rev. Biochem.* **2017**, *86*, 873−896.

(44) Koning, R. I.; Koster, A. J.; Sharp, T. H. Advances in Cryo-Electron Tomography for Biology and Medicine. *Ann. Anat.* **2018**, *217*, 82−96.

(45) Zheng, H.; Meng, Y. S.; Zhu, Y. Frontiers of in Situ Electron Microscopy. *MRS Bull.* **2015**, *40*, 12−18.

(46) Hansen, T. W.; Wagner, J. B.; Dunin-Borkowski, R. E. Aberration Corrected and Monochromated Environmental Transmission Electron Microscopy: Challenges and Prospects for Materials Science. *Mater. Sci. Technol.* **2010**, *26*, 1338−1344.

(47) Jinschek, J. R. Advances in the Environmental Transmission Electron Microscope (ETEM) for Nanoscale in Situ Studies of Gas-Solid Interactions. *Chem. Commun.* **2014**, *50*, 2696−2706.

(48) van Omme, J. T.; Wu, H.; Sun, H.; Beker, A. F.; Lemang, M.; Spruit, R. G.; Maddala, S. P.; Rakowski, A.; Friedrich, H.; Patterson, J. P.; et al. Liquid Phase Transmission Electron Microscopy with Flow and Temperature Control. *J. Mater. Chem. C* **2020**, *8*, 10781−10790.

(49) Taheri, M. L.; Stach, E. A.; Arslan, I.; Crozier, P. A.; Kabius, B. C.; LaGrange, T.; Minor, A. M.; Takeda, S.; Tanase, M.; Wagner, J. B.; et al. Current Status and Future Directions for in Situ Transmission Electron Microscopy. *Ultramicroscopy* **2016**, *170*, 86−95.

(50) van Omme, J. T.; Zakhozheva, M.; Spruit, R. G.; Sholkina, M.; Pérez Garza, H. H. Advanced Microheater for in Situ Transmission Electron Microscopy; Enabling Unexplored Analytical Studies and Extreme Spatial Stability. *Ultramicroscopy* **2018**, *192*, 14−20.

(51) Hata, S.; Honda, T.; Saito, H.; Mitsuhara, M.; Petersen, T. C.; Murayama, M. Current Opinion in Solid State & Materials Science Electron Tomography : An Imaging Method for Materials Deformation Dynamics. *Curr. Opin. Solid State Mater. Sci.* **2020**, *24*, 100850.

(52) Epicier, T.; Koneti, S.; Avenier, P.; Cabiac, A.; Gay, A. S.; Roiban, L. 2D & 3D in Situ Study of the Calcination of Pd Nanocatalysts Supported on Delta-Alumina in an Environmental Transmission Electron Microscope. *Catal. Today* **2019**, *334*, 68−78.

(53) Banjak, H.; Grenier, T.; Epicier, T.; Koneti, S.; Roiban, L.; Gay, A.-S.; Magnin, I.; Peyrin, F.; Maxim, V. Evaluation of Noise and Blur Effects with SIRT-FISTA-TV Reconstruction Algorithm: Application to Fast Environmental Transmission Electron Tomography. *Ultramicroscopy* **2018**, *189*, 109−123.

(54) Albrecht, W.; Bladt, E.; Vanrompay, H.; Smith, J. D.; Skrabalak, S. E.; Bals, S. Thermal Stability of Gold/Palladium Octopods Studied in Situ in 3D: Understanding Design Rules for Thermally Stable Metal Nanoparticles. *ACS Nano* **2019**, *13*, 6522−6530.

(55) Ren, D.; Ophus, C.; Chen, M.; Waller, L. A Multiple Scattering Algorithm for Three Dimensional Phase Contrast Atomic Electron Tomography. *Ultramicroscopy* **2020**, *208*, 112860.

(56) Kaiser, U.; Chuvilin, A. Enhanced Compositional Contrast in Imaging of Nanoprecipitates Buried in a Defective Crystal Using a Conventional TEM. *Microsc. Microanal.* **2003**, *9*, 36−41.

(57) Brown, H. G.; Ciston, J. Atomic Resolution Imaging of Light Elements in a Crystalline Environment Using Dynamic Hollow-Cone Illumination Transmission Electron Microscopy. *Microsc. Microanal.* **2020**, *26*, 623−629.

(58) Rebled, J. M.; Yedra, L.; Estradé, S.; Portillo, J.; Peiro, F. A New Approach for 3D Reconstruction from Bright Field TEM Imaging : Beam Precession Assisted Electron Tomography. *Ultramicroscopy* **2011**, *111*, 1504−1511.

(59) Bals, S.; Van Tendeloo, G.; Kisielowski, C. A New Approach for Electron Tomography : Annular Dark-Field Transmission Electron Microscopy. *Adv. Mater.* **2006**, *18*, 892−895.

(60) Adler, J.; Öktem, O. Learned Primal-Dual Reconstruction. *IEEE Trans. Med. Imaging* **2018**, *37*, 1322−1332.

(61) Pelt, D. M.; Batenburg, K. J. Fast Tomographic Reconstruction from Limited Data Using Artificial Neural Networks. *IEEE Trans. Image Process.* **2013**, *22*, 5238−5251.

(62) Pelt, D. M.; Batenburg, K. J.; Sethian, J. A. Improving Tomographic Reconstruction from Limited Data Using Mixed-Scale Dense Convolutional Neural Networks. *J. Imaging* **2018**, *4*, 128.

(63) Zhu, B.; Liu, J. Z.; Cauley, S. F.; Rosen, B. R.; Rosen, M. S. Image Reconstruction by Domain-Transform Manifold Learning. *Nature* **2018**, *555*, 487−492.

(64) Ding, G.; Liu, Y.; Zhang, R.; Xin, H. L. A Joint Deep Learning Model to Recover Information and Reduce Artifacts in Missing-Wedge Sinograms for Electron Tomography and Beyond. *Sci. Rep.* **2019**, *9*, 12803.

(65) Dong, C.; Loy, C. C.; He, K.; Tang, X. Image Super-Resolution Using Deep Convolutional Networks. *IEEE Trans. Pattern Anal. Mach. Intell.* **2016**, *38*, 295−307.

(66) Altantzis, T.; Lobato, I.; De Backer, A.; Béché, A.; Zhang, Y.; Basak, S.; Porcu, M.; Xu, Q.; Sánchez-Iglesias, A.; Liz-Marzán, L. M.; et al. Three-Dimensional Quantification of the Facet Evolution of Pt Nanoparticles in a Variable Gaseous Environment. *Nano Lett.* **2019**, *19*, 477−481.

(67) Zhuge, X.; Jinnai, H.; Dunin-Borkowski, R. E.; Migunov, V.; Bals, S.; Cool, P.; Bons, A. J.; Batenburg, K. J. Automated Discrete Electron Tomography − Towards Routine High-Fidelity Reconstruction of Nanomaterials. *Ultramicroscopy* **2017**, *175*, 87−96.

(68) Ruhlandt, A.; Töpperwien, M.; Krenkel, M.; Mokso, R.; Salditt, T. Four Dimensional Material Movies: High Speed Phase-Contrast Tomography by Backprojection along Dynamically Curved Paths. *Sci. Rep.* **2017**, *7*, 6487.

(69) De Schryver, T.; Dierick, M.; Heyndrickx, M.; Van Stappen, J.; Boone, M. A.; Van Hoorebeke, L.; Boone, M. N. Motion Compensated Micro-CT Reconstruction for in-Situ Analysis of Dynamic Processes. *Sci. Rep.* **2018**, *8*, 7655.

(70) Lucka, F.; Huynh, N.; Betcke, M.; Zhang, E.; Beard, P.; Cox, B.; Arridge, S. Enhancing Compressed Sensing 4D Photoacoustic Tomography by Simultaneous Motion Estimation. *SIAM J. Imaging Sci.* **2018**, *11*, 2224−2253.

(71) Vanrompay, H.; Buurlage, J.-W.; Pelt, D. M.; Kumar, V.; Zhuo, X.; Liz-Marzán, L. M.; Bals, S.; Batenburg, K. J. Real-Time Reconstruction of Arbitrary Slices for Quantitative and In Situ 3D Characterization of Nanoparticles. *Part. Part. Syst. Charact.* **2020**, *37*, 2000073.